Mechanisms of Redox-Coupled Proton Transfer in Proteins: Role of the Proximal Proline in Reactions of the [3Fe-4S] Cluster in *Azotobacter vinelandii* Ferredoxin I[†,‡]

Raul Camba,[§] Yean-Sung Jung,[||,⊥] Laura M. Hunsicker-Wang,[#] Barbara K. Burgess,[||] C. David Stout,[#] Judy Hirst,*[,@] and Fraser A. Armstrong*[,§]

Department of Chemistry, Oxford University, South Parks Road, Oxford, OX1 3QR, England, Department of Molecular Biology and Biochemistry, University of California, Irvine, California 92697, Department of Molecular Biology, The Scripps Research Institute, 10550 North Torrey Pines Road, La Jolla, California 92037-1083, and Medical Research Council Dunn Human Nutrition Unit, Hills Road, Cambridge, CB2 2XY, England

Received June 13, 2003; Revised Manuscript Received July 18, 2003

ABSTRACT: The 7Fe ferredoxin from *Azotobacter vinelandii* (*Av*FdI) contains a [3Fe-4S]$^{+/0}$ cluster that binds a single proton in its reduced level. Although the cluster is buried, and therefore inaccessible to solvent, proton transfer from solvent to the cluster is fast. The kinetics and energetics of the coupled electron−proton transfer reaction at the cluster have been analyzed in detail by protein-film voltammetry, to reveal that proton transfer is mediated by the mobile carboxylate of an adjacent surface residue, aspartate-15, the p*K* of which is sensitive to the charge on the cluster. This paper examines the role of a nearby proline residue, proline-50, in proton transfer and its coupling to electron transfer. In the P50A and P50G mutants, a water molecule has entered the cluster binding region; it is hydrogen bonded to the backbone amide of residue-50 and to the Asp-15 carboxylate, and it is approximately 4 Å from the closest sulfur atom of the cluster. Despite the water molecule linking the cluster more directly to the solvent, proton transfer is not accelerated. A detailed analysis reveals that Asp-15 remains a central part of the mechanism. However, the electrostatic coupling between cluster and carboxylate is almost completely quenched, so that cluster reduction no longer induces such a favorable shift in the carboxylate p*K*, and protonation of the base no longer induces a significant shift in the p*K* of the cluster. The electrostatic coupling is crucial for maintaining the efficiency of proton transfer both to and from the cluster, over a range of pH values.

Mechanisms of long-range proton transfer, and of the coupling of proton transfer to catalytic electron transfer in proteins (for example, in cytochrome *c* oxidase), are of fundamental importance in biological energy conservation (*1*−*15*). Although proton transport is widely considered to involve chains of closely spaced donors and acceptors (water molecules or amino acid side chains), relatively little is established at the atomic/molecular level about how individual transfers occur or how they are coupled to electron transfer (*16*−*18*). The generally held view is that internal water molecules are essential for mediating long-range proton transport via the Grotthus mechanism (*19*, *20*). To help understand redox-driven proton transfers at the atomic level, we have studied ferredoxin I from *Azotobacter vinelandii* (*Av*FdI),[1] a small protein that contains one [4Fe-4S]$^{2+/+}$ cluster and one [3Fe-4S]$^{+/0}$ cluster. *Av*FdI has been characterized in detail by crystallography and different spectroscopic methods (*21*−*28*). The [3Fe-4S] cluster rapidly binds a proton in the one-electron-reduced (0) level, despite the fact that it is buried approximately 8 Å below the protein surface. The exact site of proton binding has not been established, but it is most likely to be one of the cluster μ_2-sulfido ligands (*21*, *29*). Other [3Fe-4S]-containing proteins exhibit similar behavior, and there is no evidence for proton binding to the oxidized cluster (*30*, *31*). The strong dependence of cluster protonation upon cluster oxidation level, and the fact that protons can only access the cluster across a hydrophobic protein barrier, are features that may be used to construct proton-pumping devices in complex, redox-coupled, membrane-bound enzymes. Therefore, *Av*FdI is considered to be a proton-transferring module, but one that is small and simple enough to be characterized in detail by a number of discriminating investigative techniques.

Investigations of *Av*FdI by protein-film voltammetry (PFV) have allowed simultaneous measurements of the energetics and kinetics of proton-transfer reactions coupled to electron

[†] This work was supported by the EPSRC, BBSRC (43/11675), and NIH (GM48495 and GM35342).

[‡] The PDB accession numbers for the structures reported in this manuscript are 1PC4 (P50A) and 1PC5 (P50G).

* Corresponding authors. (F.A.A.) Tel: 44 1865 287182. Fax: 44 1865 272647. E-mail: fraser.armstrong@chem.ox.ac.uk. (J.H.) Tel: 44 1223 252810. Fax: 44 1223 252815. E-mail: jh@mrc-dunn.cam.ac.uk.

[§] Oxford University.

[||] University of California.

[⊥] Current address: Department of Biochemistry and Molecular Biology, Mississippi State University, Mississippi State, Mississippi 39762.

[#] The Scripps Research Institute.

[@] Medical Research Council Dunn Human Nutrition Unit.

[1] Abbreviations: *Av*FdI, *Azotobacter vinelandii* ferredoxin I; PFV, protein-film voltammetry; PGE, pyrolytic graphite edge; SHE, standard hydrogen electrode; RMSD, root-mean-square deviation.

10.1021/bi035021v CCC: $25.00
Published on Web 08/21/2003

Scheme 1: Thermodynamic Scheme for Electronation and Protonation of the [3Fe-4S] Cluster of *Av*FdI[a]

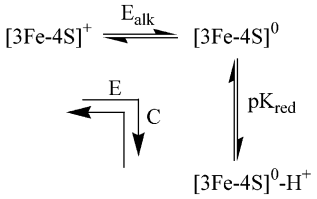

[a] There is no evidence for participation of the species $[3Fe\text{-}4S]^{1+}$-H^+. In electrochemical terminology, the cycle comprising the transformation from the oxidized cluster to the reduced protonated cluster (electron transfer followed by proton transfer), and the reverse reaction in which these events are retraced, is an ECCE reaction.

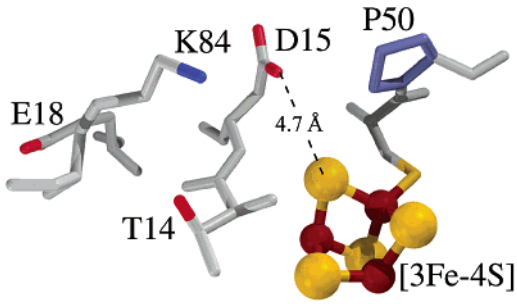

FIGURE 1: Structure of native *A. vinelandii* ferredoxin I in the vicinity of the [3Fe-4S] cluster, showing the residues that may assist in transferring a proton to the cluster, buried below the solvent accessible surface. The protein is at pH 8.5 in the oxidized form, and the figure is taken from PDB file 7FD1.

transfer (*32*−*35*). The driving force is provided by the electrode potential, and the time scale is imposed by the rate at which the potential is scanned. These studies have exploited the fact that interfacial electron exchange with protein molecules adsorbed (at up to monolayer coverage) on a pyrolytic graphite edge (PGE) electrode surface is fast. Indeed, the electron exchange constant at zero driving force, k_0, is sufficiently large that high scan rates (typically up to 100 V s^{-1}) can be used to reveal details of the electron−proton coupling kinetics (*36*−*40*). The following sequence of events (Scheme 1) has been established unambiguously: electron transfer to the cluster is followed by proton transfer from bulk water; then in the reverse reaction, electron transfer off the cluster does not occur until the proton has been released to solvent. Thus, in the reduction half cycle electron transfer drives proton transfer, whereas in the oxidation half cycle electron transfer is gated by proton transfer.

The structure of the protein in the region of the [3Fe-4S] cluster is shown in Figure 1. PFV studies with various site-directed mutants have established that proton transfer between the solvent and the cluster is mediated by the exposed carboxyl group of Asp-15 (D15), which can swing back and forth to act as a proton courier between cluster and solvent (*35*). Importantly, in contrast to other long-range proton-transfer reactions that have been studied, no water molecule is involved in this process (*6*). The mechanism is presented in Scheme 2. The kinetics of proton transfer both to and from the cluster are dependent on pH. Inward-bound proton transfer requires prior protonation of the Asp-15 carboxylate, the p*K* of which is sensitive to the oxidation level and protonation state of the cluster, and the neutralization of its charge assists its entry into the protein interior. Before electron transfer, the p*K* (pK_{ox}) of Asp-15 is 5.4, as

Scheme 2: Mechanism of Proton Transfer between Bulk Water and the [3Fe-4S] Cluster in *Av*FdI[a]

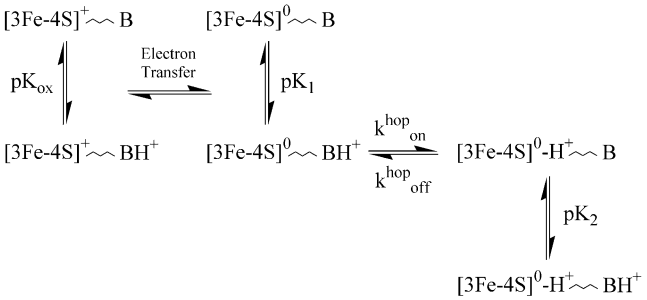

[a] Fast proton transfer to $[3Fe\text{-}4S]^0$ is pH-dependent, and the p*K* values of Asp-15 (= base, B) are sensitive to the redox and protonation states of the cluster. At low pH, Asp-15 reprotonates, inhibiting proton transfer off the cluster. For native *Av*FdI, $pK_{ox} = 5.4$, $pK_1 = 7.2$, and $pK_2 = 5.9$.

measured by NMR at 8 °C (*41*). Then, after electron transfer, the increase to 7.2 (pK_1) helps the carboxylate to capture a proton from the solvent. Molecular dynamics shows that the Asp-15 side chain is very mobile and that there are frequent approaches of the carboxylate-O to within hydrogen bonding distance of the cluster S1 atom. Conversely, outward-bound proton transfer requires prior movement of the unprotonated (negatively charged) side chain into the protein, which on electrostatic grounds is more favorable when the cluster is protonated. Outward-bound proton transfer is blocked if Asp-15 reprotonates (pK_2). Both pK_1 and pK_2 can be extracted by detailed analysis of voltammetric data: importantly, their difference (Δp*K*) is a measure of the electrostatic coupling between the cluster and Asp-15. Δp*K* should be similar to the difference between pK_1 and pK_{ox}, which reflects the effect on Asp-15 of adding an electron to the cluster.

At pH 7, proton binding to the buried cluster occurs with a bimolecular rate constant of nearly 10^{10} M^{-1} s^{-1}, a value approaching the diffusional limit for proton transfer (*42*). Replacing Asp-15 with any other residue, including glutamate, results in greatly retarded rates of proton transfer. Indeed, Asp-15 mutants exhibit kinetics 2−3 orders of magnitude slower for proton transfer both to and from the cluster, and all show similar pH-independent base-level rates. In this paper, these are termed slow mutants. In contrast, replacements of other residues, even Lys-84 which forms a salt bridge to the Asp-15 carboxylate, have little effect on the kinetics and are termed fast mutants.

Diffusion-controlled transfer of a proton to a solvent-exposed site occurs with a second-order rate constant of around 10^{11} M^{-1} s^{-1} (*42*, *43*). Therefore, there is a margin of 1 or 2 orders of magnitude remaining, by which the rate of proton transfer to the buried cluster might still be increased. We now consider the effect of possible steric restraints, and conformational flexibility in the cluster binding region, which might allow for enhanced rates of shuttling of the Asp-15 headgroup between the protein interior and the solvent or even facilitate the direct access of solvent water molecules to the cluster. As shown in Figure 1, the region around the cluster and Asp-15 includes a proline, residue Pro-50, which might be influential since mutations of proline residues are known to increase protein backbone mobility (*44*). Furthermore, analysis of the (static) crystal structure suggested that as the torsion angles of Asp-15 are rotated,

the -COOH group would come into contact with the hydrogen atoms of Cδ from Pro-50 and Cβ from Tyr-13. Together, these aspects raised the possibility that replacing Pro-50 by another residue might create a more dynamic structure, which could further enhance proton-transfer rates by making it easier for the Asp-15 side chain to swing in and out.

To examine this proposal, we have now characterized, in detail, the effect of replacing Pro-50 by alanine or glycine, on the rates and energetics of proton transfer between cluster and solvent. Proline is a highly conserved residue in sequences that bind [4Fe-4S] or [3Fe-4S] clusters, where it is proximal to a coordinating cysteine (*45*). In *Av*FdI, Pro-50 is adjacent to Cys-49, one of the [3Fe-4S] ligands.

MATERIALS AND METHODS

Preparation of the P50A and P50G Mutants of AvFdI. Site-directed mutagenesis and protein purification were carried out as reported previously (*32*). Protein samples were stored in liquid nitrogen as beaded concentrated solutions; for each set of voltammetric experiments, a bead was thawed and chromatographed by FPLC using a Mono Q column.

Crystal Structure Determination. The data for the P50A and P50G mutants were collected, integrated, and scaled using DENZO and SCALEPACK (*46*). The structures were solved using molecular replacement with the native structure and refined to 1.65 and 1.8 Å, respectively, using SHELXL (*24*, *47*). They were evaluated using PROCHECK (*48*). For P50A and P50G, 84.9 and 87.0% of the phi/psi angles were in the most favored regions, with 15.1 and 13.0% in allowed regions, respectively. The final *R* values for P50A and P50G were 15.6 and 17.9%, and R_{Free} values were 23.8 and 25.3%, respectively. The PDB deposition codes are 1PC4 (P50A) and 1PC5 (P50G).

Electrochemical Measurements. Electrochemical measurements were carried out using an AutoLab electrochemical analyzer (Eco Chemie, Utrecht, The Netherlands) equipped with modules PGStat 20 or 30, ECD, Scangen, and ADC750. Voltammograms were recorded at scan rates (ν) between 1 mV s^{-1} and 100 V s^{-1}. Data collection procedures, including *i*R compensation, Fourier transform filtering, and baseline subtraction, were carried out as described previously (*37*, *38*). A three-electrode, all-glass electrochemical cell was used (*34*, *37*). The sample compartment was maintained at 0 °C to optimize stability of the ferredoxin film and was kept anaerobic by continuous purging with a gentle stream of argon. The saturated calomel reference electrode (SCE) was connected to the sample compartment via a sidearm, ending in a Luggin capillary tip, and held at 22 °C (therefore, the cell is nonisothermal). All potentials were corrected to the standard hydrogen electrode (SHE) scale by a standard formula (*49*). Unless otherwise stated, all data are referenced to this scale. The counter electrode was a platinum wire.

The PGE working electrode had a small surface area to minimize *i*R effects and was polished before each experiment with an aqueous alumina slurry (Buehler Micropolish: 1.0 μm) and then sonicated in water. A few microliters of a 100 μM protein solution (in 60 mM mixed buffer, 0.1 M NaCl, and 200 μg mL^{-1} polymyxin) were then applied to the surface. Electroactive coverages, determined from voltammetric peak areas at slow scan rates, were typically ∼30 pmol cm^{-1}, consistent with the formation of a monolayer of protein molecules. For each measurement, the electrode potential was poised for 20 s at −650 mV, then for 10 s at an oxidizing potential, before the scan was initiated. The potential for the oxidative poise depended on the experimental pH, but it was always at least 300 mV higher than the reduction potential of the cluster to ensure that all the centers were oxidized. All chemicals were purchased from Sigma-Aldrich. Solutions were prepared using purified water of resistivity ∼18 M Ω cm (Millipore) and contained 60 mM mixed buffer (15 mM Tris, 15 mM MES, 15 mM TAPS, 15 mM acetate), 0.1 M NaCl, and 200 μg mL^{-1} polymyxin to stabilize the adsorbed protein film. The pH was adjusted with either HCl or NaOH to cover the approximate range of pH 4−10 and was measured at 0 °C before, and immediately after, each experiment.

Data Analysis and Numerical Modeling. Modeling was carried out using a finite difference procedure (*50*). Small changes in potential were simulated, and the corresponding changes in the populations of different forms of the [3Fe-4S] cluster (oxidized or reduced, protonated or deprotonated) were calculated. A simulation was assumed to have converged to the experimental condition (the analogue limit) when decreasing the potential step size resulted in no further change in the result.

Background to the Interpretation of Fast-Scan Protein-Film Voltammetry. For *Av*FdI, the order of proton and electron transfers during oxidation and reduction, as shown in Scheme 1, is defined unambiguously (*34*, *35*). In electrochemical terminology, reduction and reoxidation of the [3Fe-4S] cluster, as induced by the voltammetric cycle, is a coupled reaction of the ECCE type, where E is the electron-transfer reaction and C is the chemical reaction that is linked to it (*49*). In other words, starting with the oxidized cluster, electron transfer is followed by proton transfer, and then reoxidation requires that proton transfer precedes electron transfer. The voltammetric results are visualized and analyzed by plotting the reduction and oxidation peak potentials (Figure 2A) observed at different pH values and scan rates. Plots of the peak potential against the scan rate (on a logarithmic scale) are known as trumpet plots, and they display a wealth of information on both the kinetics and the thermodynamics of the redox reaction (*34*, *36*−*40*). Interpretation of the trumpet plots is illustrated in Figure 2B, which compares the results obtained for a fast mutant, E18Q, and a slow mutant, D15E, in each case at pH values above and below the respective cluster p*K* values. Data for the native protein are very similar to those obtained with E18Q and have been reported previously (*34*). Data for E18Q display the best fit thus far obtained for any fast variant (including native): this may be because E18 exerts a small effect on the electrostatic coupling between Asp-15 and the cluster (the distance between the carboxylate of E18 and S1 is 10.9 Å), and this complicating influence is removed when the carboxylate is changed to a carbamide.

For the condition pH > pK_{red} (no proton is transferred to the $[3Fe\text{-}4S]^0$ cluster), and commencing the cycle from the high-potential limit at which the cluster is oxidized, both the fast and the slow variants show uncomplicated electron transfer: the shape of the trumpet plot reflects only the characteristic rate constant (k_0) for electron exchange between the cluster and the electrode. In all cases, including the P50A

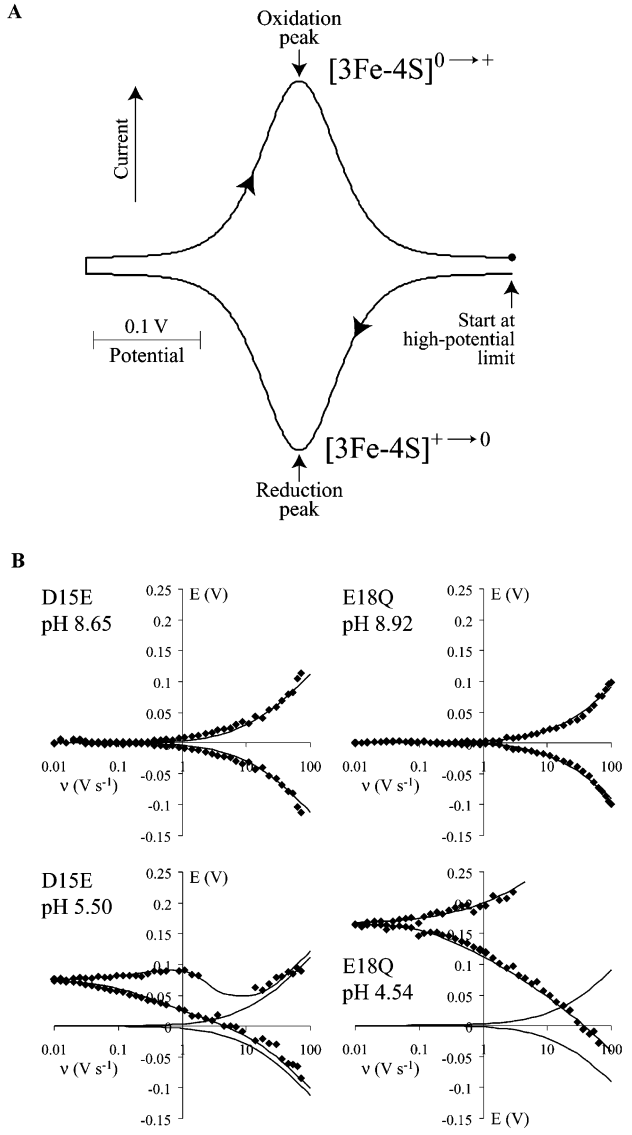

FIGURE 2: (A) Simulated cyclic voltammogram, showing how the reduction and oxidation of the [3Fe-4S] cluster is observed and measured. (B) Trumpet plots (peak potential, *E*, against scan rate, ν) comparing proton-transfer activities of E18Q (fast) and D15E (slow) variants of *Av*FdI at pH > pK_{red} and pK < pK_{red}. The data at the left-hand side of each plot correspond to the system close to equilibrium and are analogous to the results of a potentiometric measurement. On the right-hand side of each plot, the data correspond to the millisecond time domain and are kinetically controlled. For D15E, oxidation becomes gated by proton transfer, and then decoupled from it, as the scan rate is increased. Modeled peak positions are only reported if the predicted peak height is more than 20% of a theoretically shaped, reversible peak. In each case, the zero value on the potential (E) axis corresponds to the respective value of E_{alk}, i.e., the reduction potential at pH ≫ pK_{red}.

and P50G mutants discussed here, the k_0 values show that the electron transfer is sufficiently fast so that it does not interfere with either our interpretation of the mechanism or our measurements of the rates of proton transfer. In contrast, for pH < pK_{red} there are large differences in the shapes of the trumpet plots between the fast and the slow mutants. At the left-hand side of each plot (at slow scan rates), oxidation and reduction peaks are close together, and their average values give the equilibrium reduction potentials that increase, as expected, as the pH is lowered. As the scan rate is raised, the behavior becomes very dependent on the rate of the proton transfer to and from the cluster, and this is visualized most clearly with the slow mutant, D15E. First, at intermediate scan rates (1 V s^{-1} < ν < 10 V s^{-1}), the oxidation peak disappears because the electron becomes trapped on the protonated cluster: electron transfer is gated. At sufficiently fast scan rates (just above 10 V s^{-1}), it is possible to add and remove the electron before the proton can transfer to the cluster: the potential modulation out-runs the coupled chemistry so that proton transfer becomes kinetically decoupled from electron transfer. Thus, at the right-hand side of the plot for D15E, at pH < pK_{red}, the data points merge with those for pH > pK_{red}: the system now exhibits its time-resolved reduction potential—the apparent value on the millisecond time scale. In contrast, for the fast mutant E18Q, proton transfer is so fast that it cannot be decoupled, at accessible scan rates, from electron transfer (the oxidation peak does not reappear at <100 V s^{-1}), and the reduction peak potentials approach, but do not actually merge with, the data points for pH > pK_{red}. The exact shapes of the trumpet plots therefore yield rates of electron and proton transfer, as a function of potential and pH, as well as reduction potentials. Note that if a sufficiently fast cycle is commenced from the low-potential limit, at which the cluster is reduced, at pH ≪ pK_{red}, the cluster would appear silent, as no oxidative signal would be observed.

RESULTS

The overall structures of the P50A and P50G mutants are very similar to those of the native protein (see Figure 3A), with main-chain RMSD values of 0.34 and 0.38 Å, respectively. Away from the [3Fe-4S]-cluster binding region, the total structures, including the side chains of all residues except Asp-15 and residue-50, are also very similar (total RMSD values of 0.78 Å for both P50A and P50G vs the native protein). Therefore, the structural changes are confined to the immediate vicinity of residue-50.

Figure 3B shows details of the structural changes that occur in the vicinity of the [3Fe-4S] cluster for the P50A mutant. The effect of the P50G mutation is essentially identical to that of the P50A mutation, except that the methyl group is absent. The main new feature, in both mutants, is that a water molecule has been incorporated. The *B*-factor of this water molecule (number 216 in P50A and number 48 in P50G) is approximately 30 $Å^2$, so that it can be considered to be a structural water. In both P50A and P50G, it is hydrogen bonded to the amide of the mutated residue-50, the carbonyl of Glu-48, and the Asp-15 carboxylate; to accommodate this, the Asp-15 carboxylate $\chi 2$ torsion angle has changed. There is no virtually no change in the distance between cluster atom S1 and the nearest carboxylate-O atom (4.6, 4.7, and 4.8 Å in P50A, the native protein, and P50G, respectively). The position of the incorporated water molecule differs slightly between P50A and P50G, with respect to the cluster S1 atom and the closest second-shell water molecule. In P50A, it is closer to S1, although not quite within hydrogen-bonding distance (the O−S distance is 3.9 Å for P50A and 4.5 Å for P50G) but further from the closest second-shell water molecule (the O−O distance is 3.9 Å for P50A and 3.0 Å for P50G). In both sites, the water molecule is tetrahedrally coordinated: it switches its axial interaction between S1 and the adjacent water molecule, while retaining its interactions with the amide of residue-50, the carbonyl

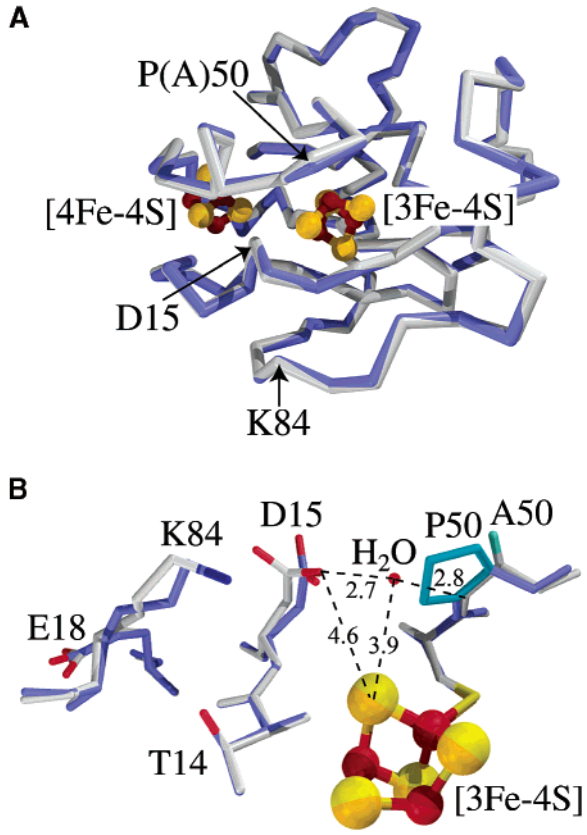

FIGURE 3: (A) Comparison of the structures of the protein backbones of the P50A mutant (PDB file 1PC4) and the native protein (PDB file 7FD1). The two structures are essentially identical. (B) Comparison of the structures of the P50A mutant and the native protein in the region of the [3Fe-4S] cluster, showing positions of the side chains, and of the water molecule that enters the structure in P50A. Distances are reported for P50A.

of Glu-48, and the carboxylate of Asp-15. Most of the water structure on the protein surface remains unchanged.

Figure 4 shows voltammograms of films of P50A obtained at slow scan rates at two different pH values. The reduction and oxidation peaks conform closely to the theoretical expectations for an immobilized redox couple displaying reversible one-electron exchange with the electrode (*37*). The peaks have half-height widths of approximately 100 mV, and the peak separation is small (approximately 10 mV). Similar results were obtained with P50G.

Figure 5 shows how the reduction potentials for P50A and P50G vary with pH. These data were obtained by taking the average of oxidation and reduction peak potentials from voltammograms recorded at scan rates slow enough to ensure equilibrium conditions (20 mV s^{-1}). Use of a slower scan rate did not alter the results. The results conform to Scheme 1 and are analyzed using eq 1

$$E_{obs} = E_{alk} + \frac{2.3RT}{nF}\log(1 + a_H{}^+/K_{red}) \qquad (1)$$

in which $a_H{}^+$ is the proton activity determined from the pH measurement (*34*). Data are now available for numerous structurally defined variants of *Av*FdI—these have also been modeled using eq 1 and are included in Figure 5. The E_{alk} and pK_{red} values are presented in Table 1. P50A and P50G display the highest potentials of all these variants, both in the region of pH where the cluster is protonated directly and

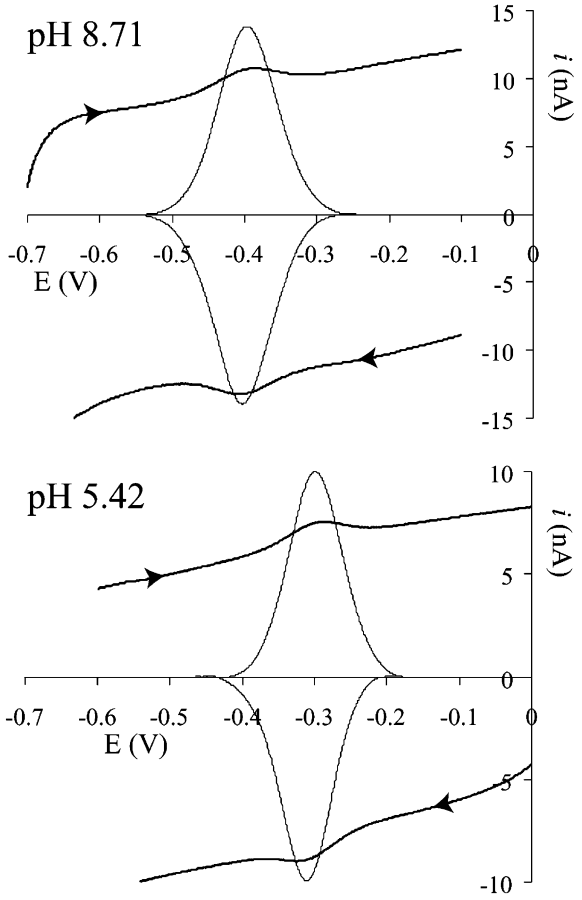

FIGURE 4: Protein-film voltammograms of the P50A mutant of *Av*FdI at a slow scan rate (10 mV s^{-1}), at pH values above and below pK_{red}. The background corrected signals are also presented; for these, the *y*-axis span represents the ideal theoretical (Nernstian) peak height. In each case, the scan was commenced from the oxidized state; temperature 0 °C; conditions as reported in Materials and Methods.

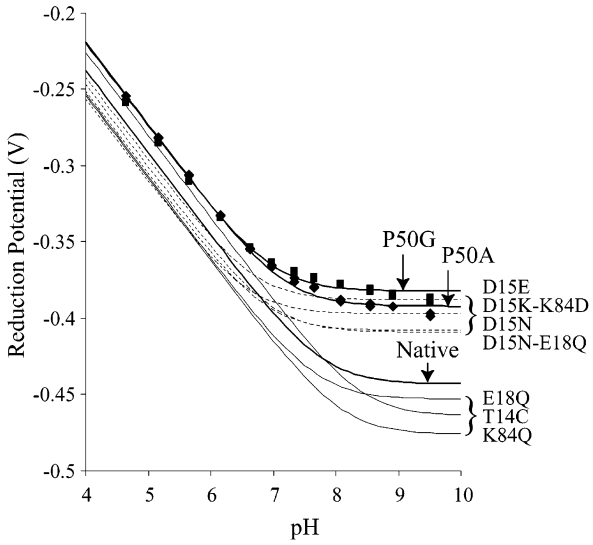

FIGURE 5: Comparison of the pH dependence of the reduction potentials of P50G, P50G, native *Av*FdI (bold), point-mutants of Asp-15 (dashed lines), and of other residues (solid lines).

(for P50G) at values above pK_{red}. Interestingly, all the other mutants that exhibit high E_{alk} values are those for which negatively charged Asp-15 has been changed to a neutral residue.

Table 1: Thermodynamic Parameters for the Reduction and Protonation of the [3Fe-4S] Clusters in Native *Av*FdI and Its Mutants

protein	pK_{red}	E_{alk} (V)
K84Q	8.1	−476
T14C	8.4	−464
E18Q	7.6	−453
native	7.8	−443
P50A	7.2	−392
P50G	7.0	−382
D15N-E18Q	7.0	−409
D15N	6.9	−408
K84Q-D15K	6.6	−397
D15E	6.7	−388

Figure 6 shows voltammograms for P50A obtained at 1, 11, and 100 V s^{-1}, for pH 8.71 and 5.42. At high pH, both the oxidation and the reduction peaks are easily observed over the entire range of scan rates, whereas at pH 5.42 the oxidation peak is still visible at 11 V s^{-1} but has vanished at 100 V s^{-1}. Similar results are obtained for P50G. This demonstrates that the P50 mutants belong to the fast category, with regard to their proton-transfer kinetics.

Figure 7 shows the trumpet plots obtained for P50A over a range of pH values. Similar data were obtained for P50G. Although P50G and P50A fall into the fast mutant category, detailed examination of these plots reveals some subtle but significant differences as compared to the other fast variants. Data were analyzed in terms of the pH-dependent model described in Scheme 2, where proton-transfer rates depend on the p*K* of the base (B, Asp-15), which varies according to the charge on the cluster. The best fits are shown as the

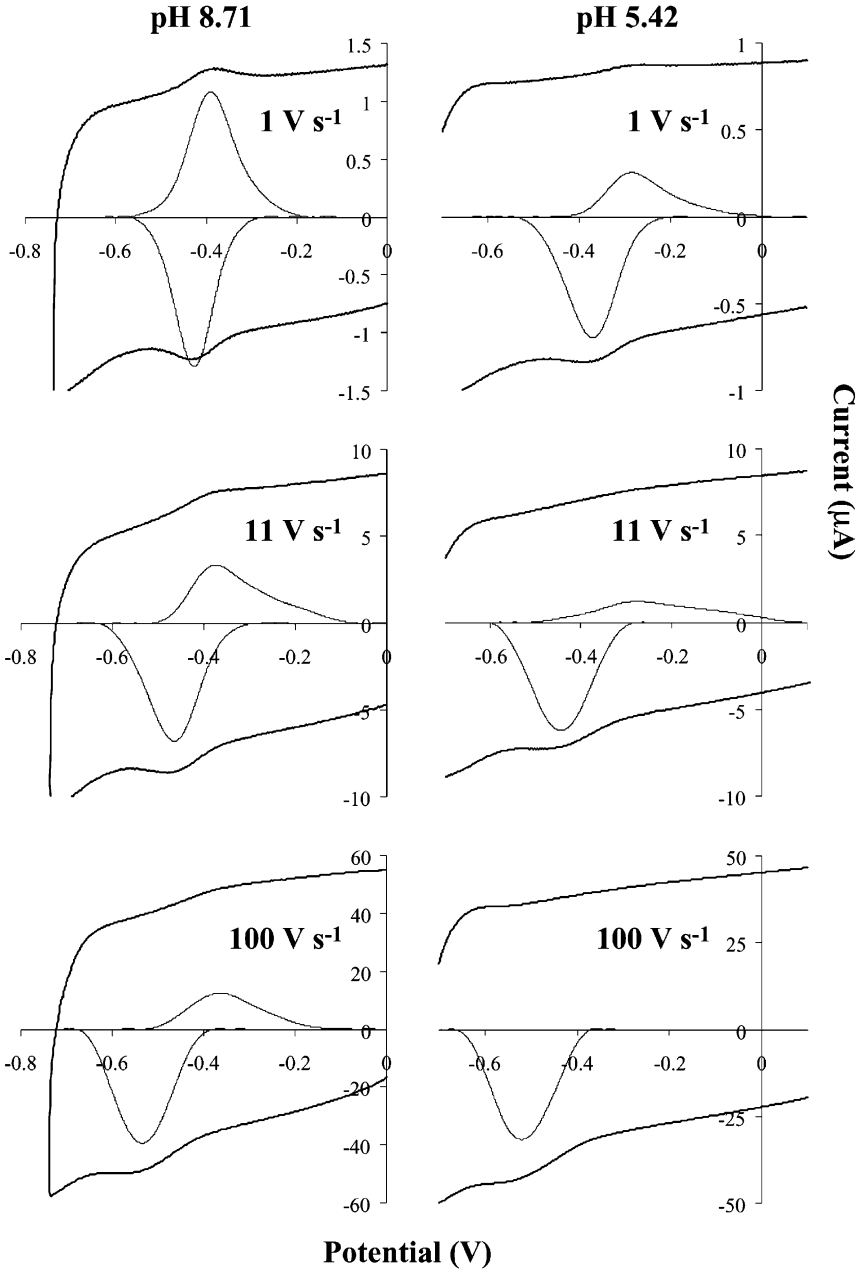

FIGURE 6: Protein-film voltammograms of the P50A mutant of *Av*FdI at scan rates 1, 11, and 100 V s^{-1}, at pH 8.71 (pH > pK_{red}) and 5.42 (pH < pK_{red}). The background corrected signals are also presented; for these, the *y*-axis span represents a perfect theoretical (Nernstian) peak height. The asymmetry observed at high scan rate, at high pH, has been discussed previously (see ref *37*) and does not affect our modeling of the proton-transfer rates. In each case, the scan was commenced from the oxidized state; temperature 0 °C; conditions as reported in Materials and Methods.

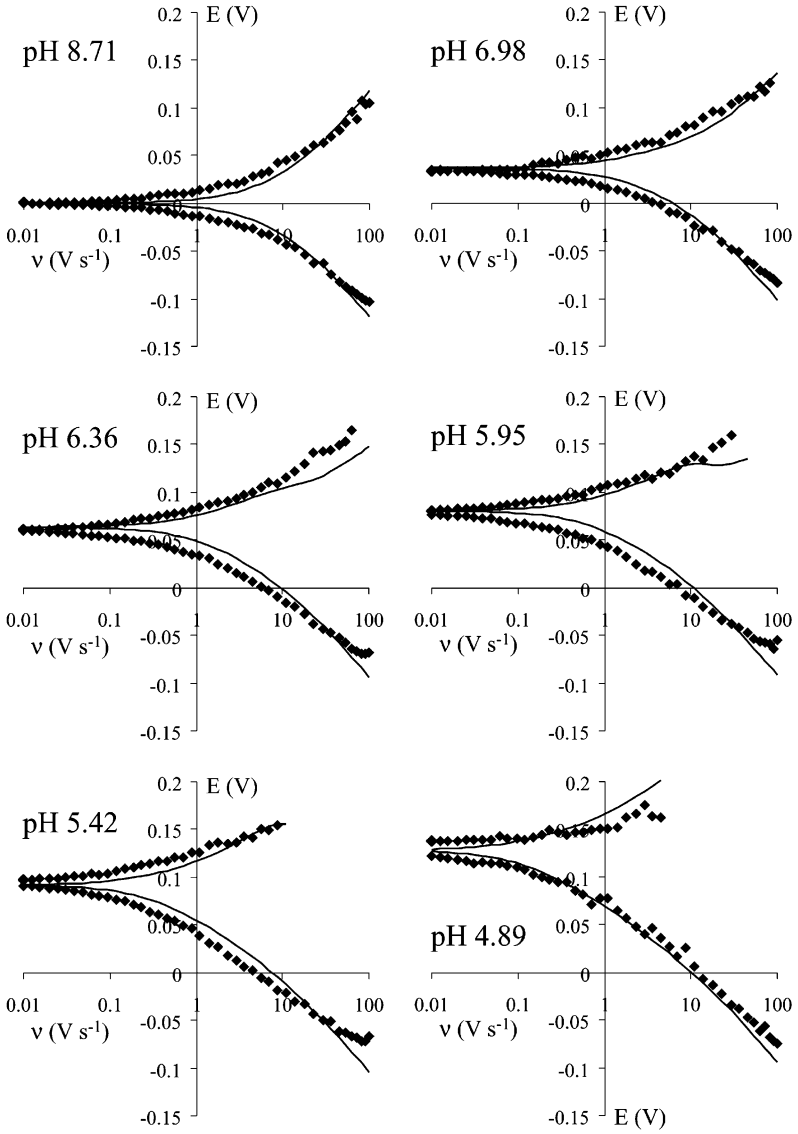

FIGURE 7: Trumpet plots (peak potential, E, against scan rate, ν) for P50A recorded over a range of pH values, with the fitted lines derived from Schemes 1 and 2 and the parameters in Table 2. Modeled peak positions are only reported if the predicted peak height is more than 20% of a theoretically shaped, reversible peak. In each case, the zero value on the potential (E) axis corresponds to the respective value of E_{alk}, i.e., the reduction potential at pH $\gg$ pK_{red}.

Table 2: Comparison between Proton Transfer Parameters Obtained for P50G and P50A and Other Fast Mutants of *Av*FdI

variant	p$K_{cluster}$ (high pH)	p$K_{cluster}$ (low pH)	k_{on} (M^{-1} s^{-1}) (pH 7)	k_{off} (s^{-1}) (pH 7)	pK_1	pK_2	ΔpK	k_{on}^{hop} (s^{-1})	k_{off}^{hop} (s^{-1})
native	7.8 ± 0.1	6.5 ± 0.1	7.9×10^9	308	7.2 ± 0.1	5.9 ± 0.1	1.3	1294 ± 100	332 ± 100
E18Q	7.7 ±0.1	6.7 ± 0.1	4.8×10^9	207	7.1 ± 0.1	6.1 ± 0.1	1.0	910 ± 90	230 ± 25
T14C	8.4 ± 0.1	7.1 ± 0.1	6.6×10^9	207	8.0 ± 0.1	6.7 ± 0.1	1.3	720 ± 100	310 ± 100
K84Q	8.1 ± 0.1	6.6 ± 0.1	9.0×10^9	232	7.4 ± 0.1	5.9 ± 0.1	1.5	1252 ± 100	250 ± 100
P50G	7.0 ± 0.1	6.7 ± 0.1	9.9×10^8	112	6.5 ± 0.1	6.2 ± 0.1	0.3	411 ± 50	118 ± 15
P50A	7.2 ± 0.1	6.8 ± 0.1	1.3×10^9	102	6.6 ± 0.1	6.2 ± 0.1	0.4	470 ± 50	118 ± 15

fitted lines in Figure 7, and analysis of the data for P50A and P50G yielded the data given in Table 2. Table 2 also includes the results obtained for other mutants.

Although the modeled lines presented in Figure 7 are the closest fit to the data that we could obtain using Scheme 2, they are not a perfect match (perhaps because of small effects from charged residues such as Glu-18). Therefore, Figure 8 shows fits to the data produced using alternative sets of parameters, to establish the acceptable boundaries of the parameters presented in Table 2 and assess the validity of our corresponding interpretations. Figure 8 shows only data recorded at pH values of 5.42 and 4.89 since these two lowest pH values are the most discriminating. First: how valid is our conclusion that ΔpK has decreased from 1.3, the value in the native protein, to 0.3 or 0.4 in P50G and P50A? Figure 8A−C displays three fits obtained when ΔpK values of 1.3 were used to fit the data from P50A. In Figure 8A, pK_1 was unchanged from its best fit value (6.6); therefore, pK_2 was decreased to 5.3. In Figure 8B, pK_2 was unchanged from its best fit value (6.2); therefore, pK_1 was increased to 7.5. In

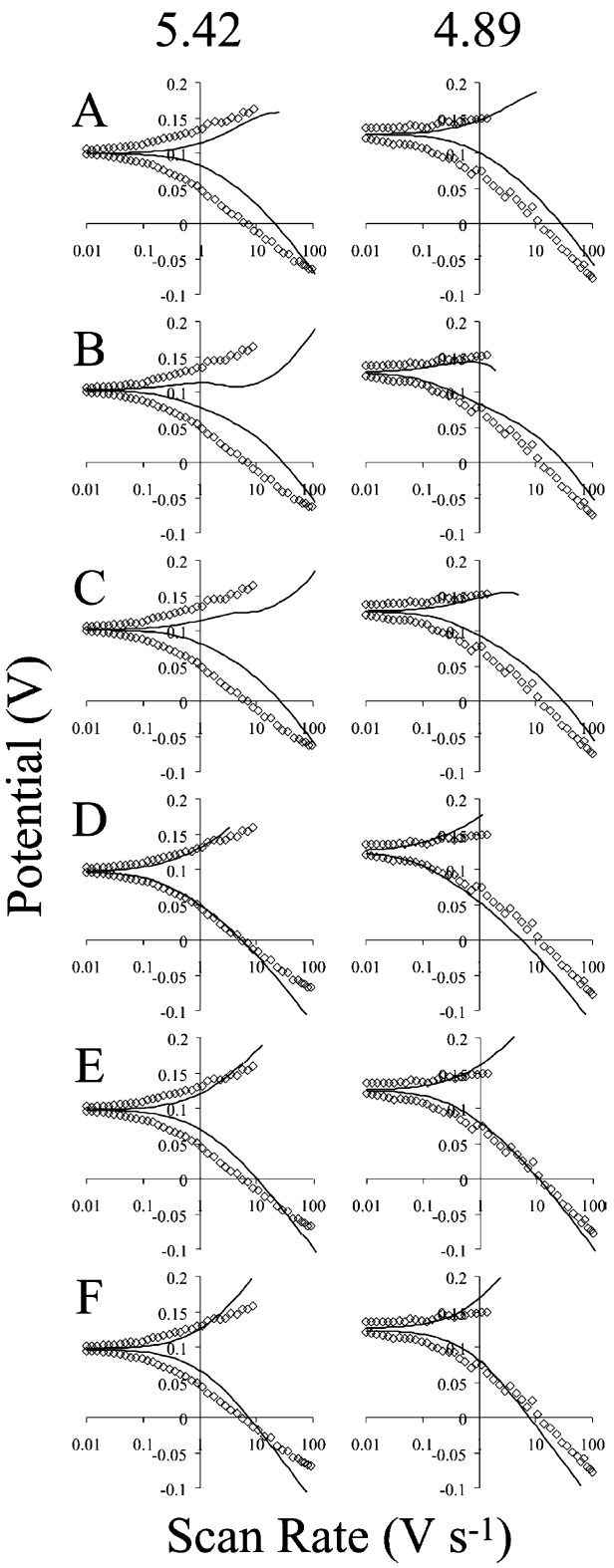

FIGURE 8: Attempts to fit the trumpet plots (peak potential, E, against scan rate, ν) for P50A using alternative sets of parameters. Only fits to the data at pH 5.42 and pH 4.89 are shown, as the lowest pH values are the most discriminating. The parameters used are as reported in Table 2, except when otherwise specified. (A) pK_1 = 6.6 (best-fit value); pK_2 = 5.3 (ΔpK = 1.3). (B) pK_1 = 7.5; pK_2 = 6.2 (best-fit value) (ΔpK = 1.3). (C) pK_1 = 7.05 (best-fit value); pK_2 = 5.75 (ΔpK = 1.3, average of pK_1 and pK_2 = 6.4 = best fit value). (D) pK_1 = pK_2 = 6.4 (average best-fit value, ΔpK = 0). (E) k_{off}^{hop} = 332 s^{-1} (the value for the native protein). (F) The mechanism for the slow mutants (Scheme 1) in which there is no participation of the base; pK_{red} = 7.2 and k_{off} = 118 s^{-1}.

Figure 8C, the average of pK_1 and pK_2 was unchanged from the best fit value (6.2); therefore, pK_1 was set to 7.05 and pK_2 to 5.75. In all three cases, the fits are markedly worse than those presented in Figure 7, with the fitted lines generally predicting plots that fall inside the data. In fact, as shown in Figure 8D, the data can be fit reasonably well by using pK_1 = pK_2, and therefore ΔpK = 0. These results demonstrate clearly the validity of our first conclusion, that the electrostatic coupling between cluster and base is quenched significantly in P50A and P50G. Second: Figure 8E shows that increasing the value of k_{off}^{hop} to match that of the native protein (332 s^{-1}), while retaining all other parameters at their best fit values, only slightly decreases the quality of the fit. Therefore, we may conclude that the proton transfer between base and cluster is not accelerated, but we cannot conclude, with certainty, that it is retarded significantly. Third: Figure 8F shows an example of an attempt to fit the data for the P50A mutant using the mechanism for the slow mutants (without the participation of a mediatory base). Only two parameters, pK_{red} and k_{off}, are required. pK_{red} is defined experimentally as 7.2 (Figure 5 and Table 1), and Figure 8F was produced using k_{off} = 118 s^{-1}. This does not produce a viable fit to the data, and the quality of the fit, over all pH values, cannot be improved by variation of k_{off}. We conclude that this simple mechanism cannot be used to describe the data from the P50G and P50A mutants.

The rates of proton transfer, and the electrostatic coupling, can now be evaluated. First, proton-transfer between the base and the cluster in the P50 mutants is certainly no faster than for the other fast mutants, and based on our best fits, it may be slower (the best fit value for k_{off}^{hop} is 2.8 times slower). However, because of the quenching of electrostatic coupling between the cluster and the base (the protonation state of the base is now much less dependent on the cluster charge), the actual rates of proton transfer to and from the cluster are altered significantly. For example, at one pH unit below the respective observed cluster pK values (7.8 for the native protein and 7.2 for P50A), k_{on} is decreased from 950 s^{-1} for the native protein to 336 s^{-1} for P50A (a ratio of 2.8), and k_{off} is decreased from 294 to 59 s^{-1} (a ratio of 5.0). At pH 7, k_{on} is decreased from 810 s^{-1} for the native protein to 134 s^{-1} for P50A (a ratio of 6.0), and k_{off} is decreased from 308 to 102 s^{-1} (a ratio of 3.0). The corresponding second-order rate constants describing cluster protonation at pH 7.0 are 8.1 $\times$ 10^9 M^{-1} s^{-1} for the native protein and 1.3 $\times$ 10^9 M^{-1} s^{-1} for P50A. Second, the difference (ΔpK) between pK_1 (when the reduced cluster is deprotonated) and pK_2 (when the reduced cluster is protonated) is much smaller for the P50 mutants ($\leq$0.4, vs 1.3 for the native protein). This quantity reflects the extent to which the mediating base (the Asp-15 carboxylate) senses the protonation state (or electronation state, see earlier) of the cluster. It is mirrored in the acid−base properties of the cluster, for which our analysis yields the virtual pK value that applies when the Asp-15 carboxylate is protonated (see Table 2).

DISCUSSION

The consequences of changing Pro-50 to glycine or alanine are subtle, yet they provide insight into the tuning of the reduction potentials and proton-transfer rates in proteins. It

is appropriate to consider first the influence on reduction potentials. Point mutations close to the [3Fe-4S] cluster in *Av*FdI result in the variation of one or more of the following (Figure 5 and Table 1): pK_{red} (the pK of the reduced cluster), E_{alk} (the limiting reduction potential at pH ≫ pK_{red}), and E_{pH} (the reduction potential at pH ≪ pK_{red}). The variation in E_{pH} is much less than in E_{alk} because for E_{pH} both a proton and an electron are transferred to the cluster (reduction is electroneutral); therefore, long-range electrostatics exert little influence. Instead, differences in E_{pH} are determined by changes in the electronic properties of the redox center. By contrast, E_{alk} represents only the addition of an electron, and so electrostatic factors, as well as the exposure of the site to solvent dipoles, may also make a significant contribution.

Previously, discussions of how protein structures control the reduction potentials of iron−sulfur clusters have tended to focus on [2Fe-2S] and [4Fe-4S] centers in which (apart from cases such as the Rieske center) only an electron is transferred into the protein (*51*−*54*). These are directly relevant to our discussions of E_{alk}. As expected, E_{alk} is increased significantly when the carboxylate of Asp-15 is replaced by neutral carbamide (D15N) or moved away from the cluster into the solvent by insertion of a -CH_2 group (D15E). It is also lowered when a nearby positive charge is removed (K84Q). Therefore, it is significant that values of E_{alk} for P50G and P50A are among the most positive of all the mutants, even though there has been no obvious change in electrostatics. Related observations have been made with the 8Fe ferredoxin from *Clostridium pasteurianum*. Mutation of residues Pro-19 and Pro-48 (adjacent to cluster-ligating Cys-18 and Cys-47), which occupy similar positions to Pro-50 in *Av*FdI, each caused a slight increase (<20 mV) in the reduction potential of the [4Fe-4S] cluster (*55*).

Some of the increase in E_{alk} resides in the electronic contribution, as gauged from the small, but noticeable, shift in E_{pH}. However, the crystal structures of P50G and P50A show that a water molecule has been incorporated. The water is buried, and although we cannot exclude the possibility that it comes into contact with both the cluster and the bulk solvent upon protein breathing, or upon a structural change due to cluster reduction, it is unreasonable to suggest that E_{alk} changes in response to increased solvation of the cluster. Instead, we conclude that the buried water molecule exerts an electrostatic effect on the cluster. The increase in E_{alk} (to ∼56 mV above the native protein) is consistent with an extra hydrogen bond to the cluster that, as is well-known, would preferentially stabilize the more reduced state, thereby raising the reduction potential (*51*−*54*). Although the water molecules in P50A and P50G are too far from S1 (at 3.9 and 4.5 Å, respectively) to form direct hydrogen bonds, the electrostatic effect of the -$O^{\delta-}$−$H^{\delta+}$ dipole is likely to be sufficient in itself. We also note that the interfacial electron-transfer rate constant (k_0) is decreased by around 50% in the Pro-50 mutants. This is consistent with an increase in reorganization energy and may therefore also result from the incorporation of the water molecule.

The original idea that led to this paper was that replacing Pro-50 by glycine or alanine would relieve possible steric constraints and introduce greater mobility to the cluster binding region, thereby making it easier for the Asp-15 carboxyl/carboxylate to approach to within hydrogen bonding distance of the cluster S1 atom. While the flexibility may indeed have increased (since access has been provided for a water molecule), the expectation for faster proton transfer between the cluster and the aspartate has not been realized: instead, the kinetics are retarded or at best unchanged. However, as discussed below, the proton-transfer rates between solvent and cluster (as opposed to between Asp-15 and cluster) have changed and provide insight into how the rates of proton transfer through proteins may be optimized.

First, the simple model used for the slow mutants, in which the proton-transfer off-rate is pH-independent, does not fit the data obtained for P50A or P50G. This confirms that the base (Scheme 2) remains a crucial part of the mechanism for P50A and P50G, as well as for the other fast mutants. The base has the effect of retarding proton transfer off the cluster at low pH (the shuttle is occupied by a proton most of the time) and retarding proton transfer to the cluster at high pH (the shuttle does not collect a proton from solvent as efficiently). However, the 2−3 orders of magnitude by which the base accelerates the rate overall far outweighs these decreases.

Second, close examination of the fast-scan voltammetry data for the Pro-50 mutants (Figure 7) shows that they behave differently to the other fast mutants (Figure 2). Fitting the data for a normal fast mutant requires that protonation of the cluster causes Asp-15 to undergo a pK shift of at least one pH unit ($\Delta pK = pK_1 - pK_2$): such a change cannot be accommodated (see Figure 8) within the data for P50G or P50A, for which the respective shifts are maximally 0.3 and 0.4 units. The same arguments apply to the cluster pK, so that the virtual pK values that apply at low pH, where Asp-15 is protonated, are almost the same as measured at equilibrium at high pH (Table 2). Therefore, we conclude that in the Pro-50 mutants, the carboxylate and cluster no longer strongly sense the protonation state of one another. This effect is very likely due to the water molecule that has been incorporated into the mutant proteins, the dipole of which may switch between different orientations as the electric field changes, thus compensating the Coulombic interaction. Although, in the absence of a D15N−P50A double mutant, we cannot eliminate the possibility that the newly incorporated water molecule substitutes for Asp-15 as the base that provides the proton relay, the pK values for the base ($pK_1 = 6.4$ and $pK_2 = 6.0$) indicate that this is unlikely to be the case.

The coupling between cluster and base was identified previously as being an important part of the proton-courier mechanism. Reduction of the cluster causes the pK of the carboxylate to increase, promoting proton capture from solvent. The neutral carboxylic group then swings toward the cluster, into the protein interior, to deliver the proton. For the reverse reaction, the protonated cluster provides a more favorable electrostatic environment for entry of the negatively charged carboxylate. Once the cluster is deprotonated it may be reoxidized, and the pK of the carboxylate drops (to $pK_{ox} = 5.5$ in the native protein), to complete the cycle of events that is driven by the electrode. In the Pro-50

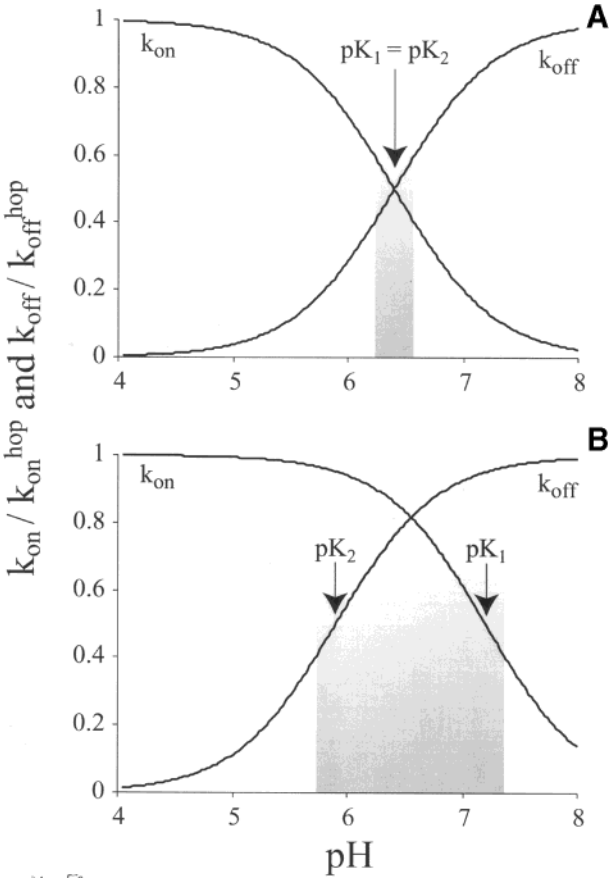

FIGURE 9: Variation with pH of the rate constants k_{on} and k_{off} (proton transfer between solvent and redox center) normalized with respect to k_{on}^{hop} and k_{off}^{hop}. At low pH, k_{on}/k_{on}^{hop} is maximized (=1) and at high pH, k_{off}/k_{off}^{hop} is maximized (=1). k_{on}/k_{on}^{hop} and k_{off}/k_{off}^{hhop} are equal to 0.5 at pK_2 and pK_1, respectively. (A) $\Delta pK = 0$; $pK_1 = pK_2 = 6.4$. (B) $\Delta pK = 1.3$; $pK_1 = 7.2$; $pK_2 = 5.9$. The shaded regions show where both k_{on}/k_{on}^{hop} and k_{off}/k_{off}^{hop} are greater than 0.4.

mutants, these electrostatic effects become inoperative, and so although the basic mechanism is still operating, it performs less efficiently. Figure 9 illustrates the effects of removing the electrostatic coupling on the rates of proton transfer between cluster and solvent (i.e., the complete transfer). Figure 9A shows how k_{on} and k_{off} (respectively, the pseudo and the true first-order rate constants, normalized with respect to k_{on}^{hop} and k_{off}^{hop}) vary with pH when there is no electrostatic coupling ($pK_1 = pK_2$). At pH = $pK_1 = pK_2$, both k_{on} and k_{off} are half their maximal value; as the pH is increased, k_{off} decreases further (although k_{on} increases), and as the pH is decreased, k_{on} decreases further (although k_{off} increases). Therefore, there is only a very limited pH range over which both k_{on} and k_{off} are high. In contrast, Figure 9B shows how k_{on} and k_{off} vary with pH when there is significant electrostatic coupling (ΔpK = 1.3). It is clear that k_{on} and k_{off} are now both optimized over a wide range of pH, and by extension, larger values of ΔpK may be employed to extend the pH range and increase the efficiency yet further. Our results demonstrate how the architecture of the cluster binding region in the native protein, containing no water molecules, provides an effective proton-transfer device that compares favorably with a more flexible and open structure allowing access of solvent molecules.

ACKNOWLEDGMENT

This paper is dedicated to our colleague, Barbara Burgess, who passed away suddenly on December 31, 2001. We thank Tom Poulos, Gareth Tilley, Kaisheng Chen, and Christopher Bonagura for helpful discussions and for carrying out some of the preparations and measurements. R.C. thanks the Mexican Government for a scholarship.

REFERENCES

1. Gennis, R. B. (1998) *Proc. Natl. Acad. Sci. U.S.A. 95*, 12747−12749.
2. Wikström, M. (1998) *Curr. Opin. Struct. Biol. 8*, 480−488.
3. Michel, H. (1998) *Proc. Natl. Acad. Sci. U.S.A. 95*, 12819−12824.
4. Lübben, M., Prutsch, A., Mamat, B., and Gerwert, K. (1999) *Biochemistry 38*, 2048−2056.
5. Pfitzner, U., Hoffmeier, K., Harrenga, A., Kannt, A., Michel, H., Bamberg, E., Richter, O. M. H., and Ludwig, B. (2000) *Biochemistry 39*, 6756−6762.
6. Gerber, N. C., and Sligar, S. G. (1994) *J. Biol. Chem. 269*, 4260−4266.
7. Takahashi, E., and Wraight, C. A. (1996) *Proc. Natl. Acad. Sci. U.S.A.* 93, 2640−2645.
8. Kuglstatter, A., Ermler, U., Michel, H., Baciou, L., and Fritzsch, G. (2001) *Biochemistry 40*, 4253−4260.
9. Mezzetti, A., Nabedryk, E., Breton, J., Okamura, M. Y., Paddock, M. L., Giacometti, G., and Leibl, W. (2002) *Biochim. Biophys. Acta 1553*, 320−330.
10. Yoshikawa, S., Shinzawa-Itoh, K., Nakashima, R., Yaono, R., Yamashita, E., Inoue, N., Yao, M., Fei, M. J., Libeu, C. P., Mizushima, T., Yamaguchi, H., Tomizaki, T., and Tsukihara, T. (1998) *Science 280*, 1723−1729.
11. Hofacker, I., and Schulten, K. (1998) *Proteins*: *Struct., Funct., Genet. 30*, 100−107.
12. Tomson, F. L., Morgan, J., Gu, G., Barquera, B., Vygodina, T. V, and Gennis, R. B. (2003) *Biochemistry 42*, 1711−1717.
13. Luecke, H., Schobert, B., Richter, H.-T., Cartailler, J. P., and Lanyi, J. K. (1999) *Science 286*, 255−260.
14. Neutze, R., Pebay-Peyroula, E., Edman, K., Royant, A., Navarro, J., and Landau, E. M. (2002) *Biochim. Biophys. Acta 1565*, 144−167.
15. Rappaport, F., and Lavergne, J. (2001) *Biochim. Biophys. Acta 1503*, 246−259.
16. Nagle, J. F., and Morowitz, H. J. (1978) *Proc. Natl. Acad. Sci. U.S.A. 75*, 298−302.
17. Williams, R. J. P. (2002) *J. Theor. Biol. 219*, 389−396.
18. Krishtalik, L. I. (2000) *Biochim. Biophys. Acta 1458*, 6−27.
19. Zheng, X., Medvedev, D. M., Swanson, J., and Stuchebrukhov, A. A. (2003) *Biochim. Biophys. Acta 1557*, 99−107.
20. Wikström, M., Verkhovsky, M. I., and Hummer, G. (2003) *Biochim. Biophys. Acta 1604*, 61−65.
21. Stout, C. D. (1989) *J. Mol. Biol. 205*, 545−555.
22. Stout, C. D. (1993) *J. Biol. Chem. 268*, 25920−25927.
23. Stout, C. D., Stura, E. A., and McRee, D. E. (1998) *J. Mol. Biol. 278*, 629−639.
24. Schipke, C. G., Goodin, D. B., McRee, D. E., and Stout, C. D. (1999) *Biochemistry 38*, 8228−8239.
25. George, S. J., Richards, A. J. M., Thomson, A. J., and Yates, M. G. (1984) *Biochem. J. 224*, 247−251.
26. Johnson, M. K., Bennett, D. E., Fee, J. A., and Sweeney, W. V. (1987) *Biochim. Biophys. Acta 911*, 81−94.
27. Stephens, P. J., Jensen, G. M., Devlin, F. J., Morgan, T. V., Stout, C. D., Martin, A. E., and Burgess, B. K. (1991) *Biochemistry 30*, 3200−3209.
28. Hu, Z. G., Jollie, D., Burgess, B. K., Stephens, P. J., and Münck, E. (1994) *Biochemistry 33*, 14475−14485.
29. Bentrop, D., Bertini, I., Borsari, M., Cosenza, Luchinat, C., and Niikura, Y. (2000) *Angew. Chem., Int. Ed. 39*, 3620−3622.
30. Breton, J. L., Duff, J. L. C., Butt, J. N., Armstrong, F. A., George, S. J., Petillot, Y., Forest, E., Schäfer, G., and Thomson, A. J. (1995) *Eur. J. Biochem. 233*, 937−946.
31. Fawcett, S. E. J., Davis, D., Breton, J. L., Thomson, A. J., and Armstrong, F. A. (1998) *Biochem. J. 335*, 357−368.
32. Shen, B., Martin, L. L., Butt, J. N., Armstrong, F. A., Stout, C. D., Jensen, G. M., Stephens, P. J., La Mar, G. N., Gorst, C. M., and Burgess, B. K. (1993) *J. Biol. Chem. 268*, 25928−25939.

33. Butt, J. N., Sucheta, A., Martin, L. L., Shen, B., Burgess, B. K., and Armstrong, F. A. (1993) *J. Am. Chem. Soc. 115*, 12587−12588.
34. Hirst, J., Duff, J. L. C., Jameson, G. N. L., Kemper, M. A., Burgess, B. K., and Armstrong, F. A. (1998) *J. Am. Chem. Soc. 120*, 7085−7094.
35. Chen, K., Hirst, J., Camba, R., Bonagura, C. A., Stout, C. D., Burgess, B. K., and Armstrong, F. A. (2000) *Nature 405*, 814−817.
36. Armstrong, F. A., Heering, H. A., and Hirst, J. (1997) *Chem. Soc. Rev. 26*, 169−179.
37. Hirst, J., and Armstrong, F. A. (1998) *Anal. Chem. 70*, 5062−5071.
38. Jeuken, L. J. C., and Armstrong, F. A. (2001) *J. Phys. Chem. B. 105*, 5271−5282.
39. Armstrong, F. A. (2002) *J. Chem. Soc., Dalton Trans.* 661−671.
40. Jeuken, L. J. C., Wisson, L.-J., and Armstrong, F. A. (2002) *Inorg. Chim. Acta 331*, 216−223.
41. Cheng, H., Grohmann, K., and Sweeney, W. (1990) *J. Biol. Chem. 265*, 12388−12392.
42. Caldin, E. F., and Gold, V. (1975) *Proton-Transfer Reactions*, Chapman and Hall, London.
43. Gutman, M., and Nachliel, E. (1995) *Biochim. Biophys. Acta 1231*, 123−138.
44. Creighton, T. E. (1993) *Proteins: Structure and Molecular Properties, 2nd ed.*, W. H. Freeman, New York.
45. Cammack, R. (1996) *Origin and Evolution of Biological Energy Conservation*, Wiley, New York.
46. Otwinowski, Z., and Minor, W. (1993) *DENZO. A file processing program for macromolecular crystallography*, Yale University, New Haven, CT.
47. Sheldrick, G. M., and Schneider, T. R. (1997) *Methods Enzymol. 277*, 319−343.
48. Laskowski, R. A., MacArthur, M. W., Moss, D. S., and Thorton, J. M. (1993) *J. Appl. Crystallogr. 26*, 283−291.
49. Bard, A. J., and Faulker, L. R. (2001) *Electrochemical Methods: Fundamentals and Applications*, 2nd ed., Wiley, New York.
50. Britz, D. (1988) *Digital Simulation in Electrochemistry*, Springer-Verlag, Berlin.
51. Li, J., Nelson, M. R., Peng, C. Y., Bashford, D., and Noodleman, L. (1998) *J. Phys. Chem. A 102*, 6311−6324.
52. Jensen, G. M., Warshel, A., and Stephens, P. J. (1994) *Biochemistry 33*, 10911−10924.
53. Langen, R., Jensen, G. M., Jacob, U., Stephens, P. J., and Warshel, A. (1992) *J. Biol. Chem. 267*, 25625−25627.
54. Warshel, A., Papazyan, A., and Muegge, I. (1997) *J. Biol. Inorg. Chem. 2*, 143−152.
55. Quinkal, I., Davasse, V., Gaillard, J., and Moulis, J. M. (1994) *Protein Eng. 7*, 681−687.

BI035021V